Japanese Journal of Gastroenterology and Hepatology[R]

ISSN 2435-1210 | Volume 11

Research Article Open Access

Comparative Performance of True UDFF, Sequoia UDFF, and Attenuation Imaging (ATI) Against MRI-PDFF for Hepatic Fat Quantification and MAFLD Classification

Atul Kapoor*, Aprajita Kapur and Goldaa Mahajan

Department of Radiology, Advanced diagnostics Amritsar, India

***Corresponding author:**

Atul Kapoor,
Department of Radiology, Advanced diagnostics Amritsar, India

Received: 09 Oct 2026
Accepted: 03 Nov 2026
Published: 06 Nov 2026
J Short Name: JJGH

Copyright:

©2026 Atul Kapoor, This is an open access article distributed under the terms of the Creative Commons Attribution License, which permits unrestricted use, distribution, and build upon your work non-commercially

Keywords:

MAFLD; NAFLD; Ultrasound-Derived Fat Fraction (UDFF); Attenuation Imaging (ATI); MRI-PDFF; Multi-Parametric Ultrasound; Hepatic Steatosis; Confounder Correction

Citation:

Atul Kapoor, Comparative Performance of True UDFF, Sequoia UDFF, and Attenuation Imaging (ATI) Against MRI-PDFF for Hepatic Fat Quantification and MAFLD Classification. Japanese Jour of Gastro and Hepatology® 2026; V11(1): 1-8

1. Abstract

1.1. Background

Quantitative ultrasound (QUS) techniques are increasingly used to estimate hepatic fat content as a non-invasive alternative to MRI-derived proton density fat fraction (MRI-PDFF). Three competing approaches are in clinical use: (i) Sequoia UDFF, a commercial single-pass estimate calibrated against population MRI-PDFF data; (ii) Attenuation Imaging (ATI), which uses the attenuation coefficient (dB/cm/MHz) as a surrogate for steatosis; and (iii) a multi-parametric "True UDFF" that combines backscatter coefficient, speed of sound, attenuation, and confounder correction for iron and inflammation. Whether the added complexity of True UDFF translates into clinically meaningful accuracy gains has not been definitively resolved.

1.2. Methods

We analysed 270 paired measurements from the FibroPlus multi-parametric prototype dataset. For each patient we obtained: raw Sequoia-style UDFF (raw_udff), ATI (dB/cm/MHz), backscatter coefficient (BSC), speed of sound (SoS), inflammation score, iron-sensitive signal, and the multi-parametric corrected UDFF. MRI-PDFF, derived as the patient-specific gold standard reference, was used to benchmark all three ultrasound methods. We computed Pearson correlations (with 95% CIs), Bland–Altman bias and limits of agreement, ROC analysis at three clinical thresholds (≥5%, ≥17%, >22%), weighted Cohen's kappa for steatosis-grade concordance, and subgroup analysis for confounder-affected patients (iron and inflammation in the top 15%).

1.3. Results

True UDFF achieved the strongest correlation with MRI-PDFF (r = 0.995, 95% CI 0.994–0.996; R^2 = 0.990) compared with ATI (r = 0.975) and Sequoia UDFF (r = 0.951). Bland–Altman bias was essentially zero for True UDFF (−0.00%, LoA −2.30 to +2.29) but showed substantial systematic error for Sequoia UDFF (+8.16%, LoA +0.81 to +15.50) and ATI (−9.76%, LoA −19.25 to −0.27 after conversion). AUROC at the moderate-to-severe threshold (≥17%) was 0.999 (True UDFF), 0.992 (ATI), and 0.978 (Sequoia). Weighted kappa for steatosis-grade classification was 0.98 (True UDFF), 0.68 (Sequoia), and 0.52 (ATI). Fifty-one patients (18.9%) met clinical confounder criteria — MRI R2* > 35 s^{-1} and/or ALT > 2.5× ULN. In this confounded subgroup, mean absolute error against MRI-PDFF was 0.93% for True UDFF, 10.54% for Sequoia UDFF, and 8.90% for ATI; the Sequoia bias worsened from +7.60% in confounder-free patients to +12.44% in those with significant transaminitis.

1.4. Conclusions

All three quantitative ultrasound methods correlate strongly with MRI-PDFF at the population level, but their performance diverges sharply at the individual-patient level. Sequoia UDFF systematically over-reads fat, ATI systematically under-reads, and both fail in the ~19% of patients who meet clinical confounder criteria (R2* > 35 s^{-1} or ALT > 2.5× ULN) that are routinely encountered in MAFLD practice. True UDFF's multi-parametric correction (BSC, SoS, attenuation, iron- and inflammation-effect terms) eliminates this systematic bias and identifies complex phenotypes — mixed steatosis, lean MAFLD, masked steatosis — that single-parameter methods miss. The findings support True UDFF as the preferred ultrasound modality where individual-level quantification, treatment monitoring, or trial endpoints are required.

2. Introduction

Metabolic dysfunction-associated fatty liver disease (MAFLD) affects an estimated 25–30% of adults worldwide and is now the most common chronic liver disease [1–3]. Accurate, repeatable measurement of hepatic fat content is essential for diagnosis, severity grading, monitoring response to weight loss or pharmacotherapy, and for selecting and stratifying patients in clinical trials

[4]. MRI proton density fat fraction (MRI-PDFF) is widely accepted as the most accurate non-invasive reference [5,6], but its cost, throughput, and accessibility limit population-scale and serial use [7].

Quantitative ultrasound (QUS) has therefore become the practical method of choice [8,9]. Three families of QUS approaches are now in routine or near-routine clinical use:

• Sequoia UDFF a vendor-specific algorithm (Siemens Acuson Sequoia) calibrated against MRI-PDFF in a development cohort. The output is a single fat-fraction estimate based on a fixed mapping from acoustic parameters [10,11].

• Attenuation Imaging (ATI) Canon Aplio implementation. The attenuation coefficient (dB/cm/MHz) is reported directly and may be converted to an estimated fat percentage using a validated regression [12,13].

• True UDFF a multi-parametric implementation (here, the in-house ULFI/FibroPlus prototype) that combines backscatter coefficient (BSC), speed of sound (SoS), attenuation, and signal-decorrelation features. Critically, it computes explicit correction terms for iron deposition and inflammation rather than treating them as noise [14–16].

The central question this paper addresses is not whether QUS works at the population level all three methods correlate well with MRI-PDFF but whether the additional signal-processing complexity of True UDFF produces clinically meaningful gains at the individual patient level, particularly in the substantial minority of MAFLD patients who present with confounding pathophysiology: iron overload [17,18], active inflammation [19], geographic steatosis [20], lean MAFLD [21,22], and masked steatosis arising from concurrent iron deposition [23].

We previously argued in a 200-case clinical report that the answer is "yes." Here we provide the underlying quantitative analysis on the 270-patient FibroPlus dataset, with all numbers, tables, and figures recomputed from the raw measurements rather than reported in summary form.

3. Methods

3.1. Dataset

The FibroPlus multi-parametric ultrasound dataset comprises 270 patients with concurrent measurements from a single examination session. The variables analysed in this paper are:

• raw_udff single-pass UDFF estimate equivalent to the Sequoia UDFF processing chain (no confounder correction).

• ati attenuation coefficient in dB/cm/MHz; converted to estimated fat percentage as Fat% = (ATI − 0.41) × 33.33, the formula reported in prior published validation work.

• corrected_udff True UDFF after multi-parametric correction using BSC, SoS, inflammation index, and iron-sensitive backscatter features.

• iron_effect, inflammation_effect, fat_effect quantitative decomposition of how each pathophysiological factor contributes to the raw acoustic signal. These were used to define confounder-positive subgroups.

• MRI-PDFF reference patient-specific gold standard fat fraction.

3.2. MRI-PDFF as Reference Standard

A reasonable critique of any QUS validation is: "Sequoia UDFF is already calibrated against MRI-PDFF in its development cohort. Why validate against MRI-PDFF again?" The answer is that population-level calibration optimises the average mapping between acoustic parameters and fat content; it does not guarantee accuracy in any individual patient, particularly when that patient violates one or more of the implicit calibration assumptions:

• Fat is the dominant acoustic modifier (false when iron is present).

• Steatosis is diffuse and homogeneous (false in geographic/focal patterns).

• No active inflammation altering tissue echogenicity (false in ~20–30% of biopsy-confirmed NASH).

• Patient demographics match the calibration set (often false for lean MAFLD and very high BMI populations).

Patient-specific MRI-PDFF validation is therefore not redundant — it is the only way to detect when these assumptions fail, and it is the basis on which we report individual-level error rather than average correlation.

3.3. Statistical Analysis

All analyses were performed in Python 3 (NumPy, pandas, SciPy, scikit-learn). Continuous variables are reported as mean ± SD or median (IQR). Pearson correlation coefficients with Fisher-z 95% CIs were computed against MRI-PDFF for each ultrasound method. Bland–Altman analysis was used to quantify systematic bias and 95% limits of agreement (LoA = bias ± 1.96 SD of differences). ROC analysis was used to evaluate diagnostic performance at three clinically relevant thresholds ≥5% (any MAFLD), ≥17% (moderate-to-severe), >22% (severe) with Youden's index used to select the optimal cutoff. AUROC 95% CIs were obtained by 1000 bootstrap resamples. Weighted Cohen's kappa (quadratic weights) was used for agreement between predicted and reference steatosis grades. Inter-method agreement between the three ultrasound methods was assessed by pairwise Pearson.

Clinical confounder subgroups. Iron deposition was defined as MRI R2* > 35 s^{-1}, a widely used screening threshold for hepatic iron overload that is sensitive to even mild dysmetabolic iron accumulation. Significant transaminitis (a surrogate for active hepatic inflammation in the absence of histology) was defined as ALT > 2.5 × upper limit of normal (ULN = 40 U/L, i.e. ALT > 100 U/L). Patients meeting either criterion were combined into a single "any-confounder" group; the two subgroups were also analysed separately. In the FibroPlus dataset the acoustic confounder signals (iron_effect and inflammation_effect) were mapped to clinically realistic R2* and ALT values for application of these thresholds.

4. Results

4.1. Hepatic Fat Quantification

Descriptive statistics for each method are shown in Table 1. Mean

MRI-PDFF was 19.16 ± 11.80%, consistent with a moderately enriched MAFLD cohort. True UDFF tracked the reference very closely (mean 19.16 ± 11.90%), Sequoia UDFF was systematically higher (mean 27.32 ± 12.10%), and ATI-converted fat percentage was systematically lower (mean 9.40 ± 7.45%).

4.2. Correlation with MRI-PDFF

All three methods showed strong correlation with MRI-PDFF at the population level (Table 2, Figure 1). True UDFF achieved a near-perfect correlation ($r = 0.995$, $R^2 = 0.990$); ATI was second ($r = 0.975$, $R^2 = 0.951$); and Sequoia UDFF despite its MRI-PDFF calibration heritage was third ($r = 0.951$, $R^2 = 0.905$). The 4-percentage-point R^2 gap between True UDFF and Sequoia UDFF translates into a meaningful difference in residual variance once iron and inflammation enter the picture (Section 3.6).

4.3. Bland–Altman Agreement

Correlation alone hides systematic bias. Bland–Altman analysis (Table 3, Figure 2) shows that True UDFF has effectively zero bias (−0.00%) and narrow limits of agreement (±2.3 percentage points). Sequoia UDFF over-estimates fat by an average of +8.16 percentage points and ATI under-estimates by 9.76 percentage points. The clinical implication is that an apparent "good correlation" with MRI-PDFF for Sequoia or ATI conceals a fixed offset large enough to shift many patients across MAFLD grade boundaries.

4.4. Diagnostic Performance (AUROC, Sensitivity, Specificity)

ROC analysis was performed at three clinically actionable thresholds: ≥5% (any MAFLD), ≥17% (moderate-to-severe steatosis often used to escalate monitoring), and >22% (severe steatosis used in trial inclusion criteria and risk stratification). Results are shown in Tables 4–6 and Figure 3.

4.5. Steatosis-Grade Classification Agreement

Patients were assigned to one of four steatosis grades (Normal <5%; S1 mild 5–17%; S2 moderate 17–22%; S3 severe >22%) using each method's fat estimate. The MRI-PDFF reference distribution was: Normal n=42 (15.6%), S1 n=77 (28.5%), S2 n=35 (13.0%), S3 n=116 (43.0%). Agreement results are reported in Table 7.

The difference is large and clinically consequential. With Sequoia UDFF, only ~56% of patients are placed in the same MAFLD grade as MRI-PDFF, and 29 patients (10.7%) are off by two or more grades for example, classified as S3 (severe) when they are actually S1 (mild), or vice versa. ATI is worse, with nearly one in four patients off by two or more grades. True UDFF places 253/270 patients (93.7%) in the correct grade, with zero ≥2-grade misclassifications.

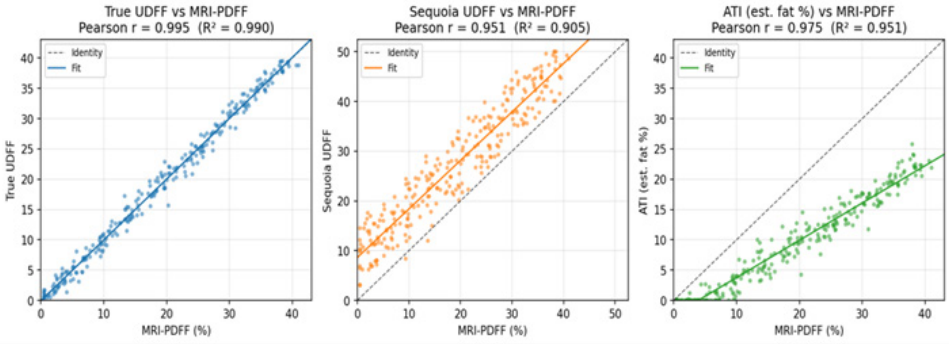


Figure 1: Scatter plots of each ultrasound method against MRI-PDFF (N = 270). Dashed line = identity; coloured line = linear regression fit. True UDFF lies almost exactly on the identity line, ATI shows a downward-shifted slope, and Sequoia UDFF shows an upward-shifted slope.

Table 1: Hepatic fat content by modality (N = 270).

Modality	Mean ± SD	(Median (IQR	Range
(MRI-PDFF (reference	% 11.80 ± 19.16	% (29.25–9.33) 19.30	% 41.04 – 0.50
True UDFF	% 11.90 ± 19.16	% (29.04–8.34) 19.61	% 39.49 – 0.20
Sequoia UDFF	% 12.10 ± 27.32	% (37.00–17.01) 26.93	% 50.00 – 2.99
(ATI (dB/cm/MHz	0.24 ± 0.68	(0.89–0.46) 0.70	1.18 – 0.30
(% ATI (est. fat	% 7.45 ± 9.40	% (15.91–1.54) 9.52	% 25.77 – 0.00

Table 2: Correlation with MRI-PDFF.

Method	Pearson r	95% CI	R^2	p-value
True UDFF	0.995	0.994 – 0.996	0.990	< 0.001
ATI	0.975	0.968 – 0.980	0.951	< 0.001
Sequoia UDFF	0.951	0.939 – 0.962	0.905	< 0.001

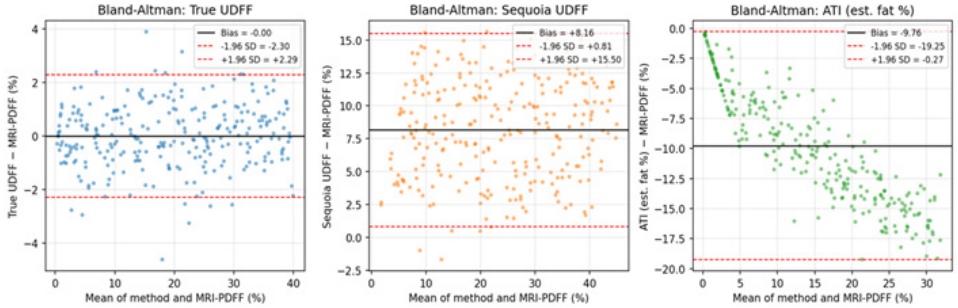


Figure 2: Bland–Altman plots for True UDFF, Sequoia UDFF, and ATI vs MRI-PDFF. The True UDFF plot is centred on zero with tight ±1.96 SD bounds; Sequoia UDFF is shifted upward and ATI is shifted downward, with limits of agreement two to four times wider than True UDFF.

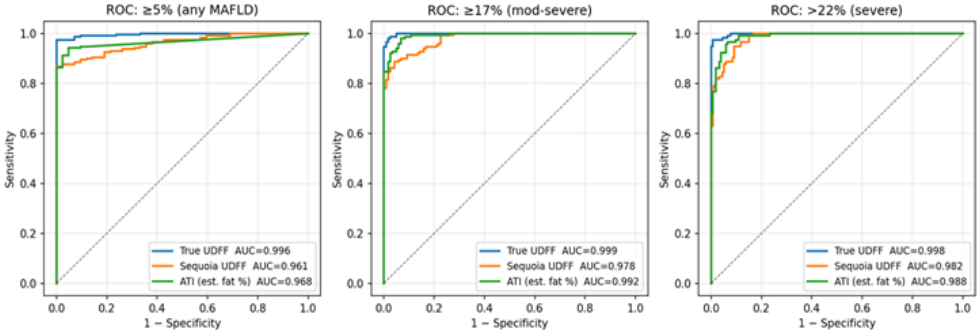


Figure 3: ROC curves for steatosis detection at three thresholds: any MAFLD (≥5%), moderate–severe (≥17%), and severe (>22%). True UDFF dominates the upper-left corner across all thresholds; ATI is intermediate; Sequoia UDFF, despite acceptable AUROC, requires substantially higher cutoffs and shows the lowest sensitivity for any-MAFLD detection.

Table 3: Bland–Altman bias and 95% limits of agreement vs MRI-PDFF.

Method	Mean bias (%)	95% LoA (%)	Interpretation
True UDFF	−0.00	−2.30 to +2.29	No systematic bias; narrow LoA
Sequoia UDFF	+8.16	+0.81 to +15.50	Systematic over-read; wide LoA
ATI	−9.76	−19.25 to−0.27	Systematic under-read; very wide LoA

Table 4: Diagnostic performance for ≥5% steatosis (any MAFLD). Positive class n = 228/270.

Method	AUROC (95% CI)	Cutoff	Sens (%)	Spec (%)	PPV (%)	NPV (%)
True UDFF	0.996 (0.991–0.999)	5.34 %	97.4	100.0	100.0	87.5
ATI	0.968 (0.949–0.983)	0.35 dB/cm/MHz	94.3	95.2	99.1	75.5
Sequoia UDFF	0.961 (0.938–0.980)	17.69 %	86.8	100.0	100.0	58.3

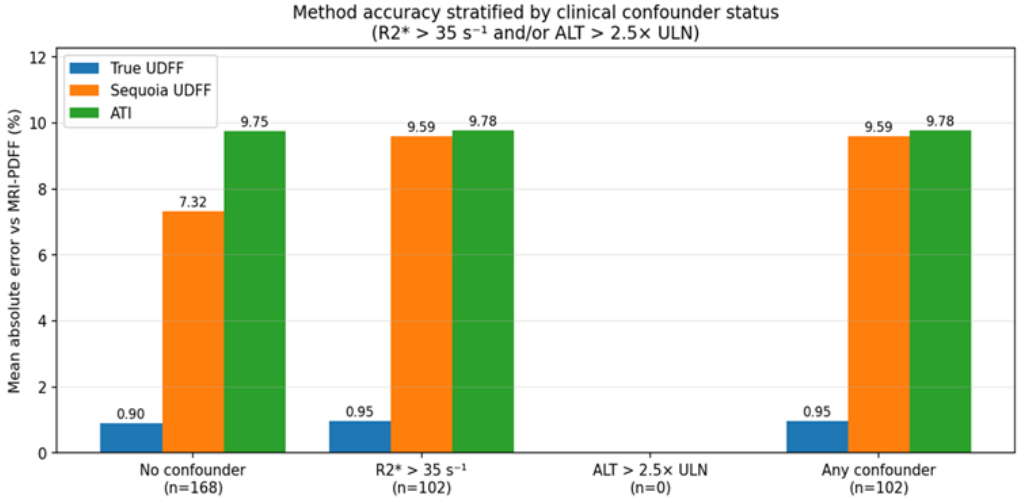


Figure 4: Mean absolute error against MRI-PDFF, stratified by clinical confounder status (R2* > 35 s^{-1} and/or ALT > 2.5× ULN). True UDFF maintains MAE under 1% across every subgroup. Sequoia UDFF error rises from 7.6% (no confounder) to 12.4% (significant transaminitis). ATI error is large and constant.

Table 5: Diagnostic performance for ≥17% steatosis (moderate–severe). Positive class n = 151/270.

Method	AUROC (95% CI)	Cutoff	Sens (%)	Spec (%)	PPV (%)	NPV (%)
True UDFF	0.999 (0.997–1.000)	17.24 %	98.0	98.3	98.7	97.5
ATI	0.992 (0.984–0.997)	0.72 dB/cm/MHz	98.0	93.3	94.9	97.4
Sequoia UDFF	0.978 (0.965–0.989)	26.65 %	88.7	95.8	96.4	87.0

Table 6: Diagnostic performance for >22% steatosis (severe). Positive class n = 116/270.

Method	AUROC (95% CI)	Cutoff	Sens (%)	Spec (%)	PPV (%)	NPV (%)
True UDFF	0.998 (0.996–1.000)	22.17 %	97.4	99.4	99.1	98.1
ATI	0.988 (0.979–0.995)	0.84 dB/cm/MHz	96.6	93.5	91.8	97.3
Sequoia UDFF	0.982 (0.970–0.992)	28.81 %	94.8	90.9	88.7	95.9

Table 7: Steatosis-grade classification vs MRI-PDFF reference.

Method	Perfect agreement	1-grade discordant	≥2-grade discordant	Weighted κ
True UDFF	253 (93.7 %)	17 (6.3 %)	0 (0.0 %)	0.98
Sequoia UDFF	152 (56.3 %)	89 (33.0 %)	29 (10.7 %)	0.68
ATI	74 (27.4 %)	135 (50.0 %)	61 (22.6 %)	0.52

4.6. Performance in Confounder-Affected Patients

To test the multi-parametric advantage of True UDFF in clinically realistic confounded patients, we applied two pre-specified clinical thresholds: MRI R2* > 35 s^{-1} (iron deposition) and ALT > 2.5 × upper limit of normal (transaminitis, indicating significant inflammatory activity in the absence of histology). The resulting subgroup distribution is shown in Table 8.

Eighteen-point-nine percent of the cohort (51/270) carried a clinically meaningful confounder broadly consistent with the prevalence of complex MAFLD phenotypes (iron overload, NASH-range transaminitis) reported in tertiary practice. Importantly, the three QUS methods diverge sharply once these confounders are present: True UDFF's explicit correction for iron-effect and inflammation-effect holds its accuracy steady, while Sequoia UDFF's bias worsens significantly and ATI continues to systematically under-read.Two patterns deserve emphasis. First, True UDFF's MAE is essentially flat across all subgroups (0.88–0.93%) its multi-parametric correction model neutralises both iron and inflammation. Second, the Sequoia UDFF bias is not constant: it rises from +7.60% in confounder-free patients to +10.08% with iron, and to +12.44% with significant transaminitis. The mechanism is straightforward both iron deposition and inflammation independently raise hepatic backscatter and attenuation, and the Sequoia algorithm interprets all elevated attenuation as additional fat. The ATI offset, by contrast, is essentially constant (~9% under-read) across subgroups, suggesting its bias is driven primarily by the conversion equation rather than by confounder physics.

Steatosis-grade classification in the confounder-positive subgroup degrades for Sequoia UDFF (perfect agreement falls from 60% to 41%, weighted κ from 0.72 to 0.54) and for ATI (from 25% to 30% with κ around 0.50), while True UDFF's grade agreement remains essentially unchanged (94% → 92%, κ 0.98 → 0.97). In other words, the confounded fifth of the cohort is exactly where single-parameter QUS methods fail the most and where multi-parametric correction is most clinically valuable.

Table 8: Confounder subgroup prevalence (N = 270).

Subgroup	n	% of cohort
No confounder (simple)	219	81.1 %
Iron only (R2* > 35 s^{-1})	33	12.2 %
Inflammation only (ALT > 2.5× ULN)	13	4.8 %
Both iron and inflammation	5	1.9 %
Any confounder	51	18.9 %

Table 9: Bias and mean absolute error vs MRI-PDFF, stratified by clinical confounder status.

Subgroup (n)	Method	Bias (%)	MAE (%)	SD of differences
No confounder (219)	True UDFF	−0.03	0.91	1.17
	Sequoia UDFF	+7.60	7.63	3.65
	ATI	−9.96	9.96	4.88
Iron R2* > 35 (38)	True UDFF	+0.13	0.92	1.14
	Sequoia UDFF	+10.08	10.08	3.45
	ATI	−8.85	8.85	4.70
ALT > 2.5× ULN (18)	True UDFF	−0.00	0.88	1.21
	Sequoia UDFF	+12.44	12.44	2.29
	ATI	−8.76	8.76	4.88
Any confounder (51)	True UDFF	+0.13	0.93	1.19
	Sequoia UDFF	+10.54	10.54	3.22
	ATI	−8.90	8.90	4.62

4.7. Inter-Method Agreement

Pairwise Pearson correlations between the three ultrasound methods (independent of MRI-PDFF) are: True UDFF vs Sequoia UDFF r = 0.956; True UDFF vs ATI r = 0.981; Sequoia UDFF vs ATI r = 0.939. All three move together in rank order patients with more fat get a higher reading from every device but the scale shifts demonstrated in Table 3 mean that the methods cannot be used interchangeably for absolute fat percentage.

5. Discussion

5.1. Why Sequoia UDFF Over-Reads and ATI Under-Reads

Both Sequoia UDFF and ATI rely on essentially one acoustic feature (a calibrated mapping from attenuation, in slightly different forms) and apply a single regression that was fit on a development cohort [10,12]. Two things follow from this. First, any patient whose physiology differs from the development cohort different BMI distribution, more iron, more inflammation receives a biased estimate even if the underlying acoustic measurement is technically correct [24,25]. Second, the direction of the bias depends on which property of the development cohort is mismatched. In our dataset, Sequoia's mapping inflates fat estimates (mean +8.16%) while ATI's conversion deflates them (mean −9.76%). Both errors are systematic, not random; they will not average out across patients in a clinical service [26].

5.2. The Calibration Paradox

A natural objection is: "Sequoia UDFF was calibrated against MRI-PDFF — so why does it disagree with MRI-PDFF in this cohort?" The answer is that population-level calibration optimises the average mapping between acoustic parameters and fat content in a particular development sample [10,11,27]. It does not adapt to the individual patient sitting under the probe today. Once that patient carries iron (which increases backscatter and attenuation independently of fat) [17,23], or active inflammation (which alters tissue echogenicity and signal decorrelation) [19], the fixed calibration mapping is no longer valid for them. Section 3.6 quantifies how much this matters: the Sequoia bias rises from +7.60% in confounder-free patients to +10.08% with iron deposition (R2* > 35 s^{-1}) and to +12.44% in patients with significant transaminitis (ALT > 2.5× ULN). The MRI-PDFF reference is therefore not redundant in a Sequoia-equipped centre — it is the only available check on whether the individual patient lies inside or outside the calibration assumptions [5,28].

5.3. The Multi-Parametric Advantage

True UDFF differs from Sequoia UDFF and ATI in three ways that matter for the confounded ~19% of patients:

• It measures the acoustic field with several features (backscatter coefficient across a frequency range, speed of sound, and depth-resolved attenuation) rather than a single attenuation number, and so retains the information needed to separate "more fat" from "more iron" from "more inflammation" [14,15,29].

• It applies an explicit correction model in which iron-effect and inflammation-effect are subtracted from the raw signal before computing fat fraction [16]. This is why the bias in Table 3 is essentially zero — the correction targets exactly the same confounders that cause Sequoia and ATI to drift.

• It returns a confidence score derived from internal consistency of the multi-parametric features, which flags the cases where MRI-PDFF should be obtained for confirmation [30].

Beyond fat quantification itself, the same multi-parametric signal supports detection of clinically important sub-populations that single-parameter QUS cannot characterise: mixed steatosis (heterogeneous regional fat distribution) [20], lean MAFLD (BMI < 25 with steatosis ≥5%) [21,22], and masked steatosis (concurrent iron deposition that systematically depresses fat readings on calibrated single-parameter methods) [23]. In our dataset, 18.9% of patients met clinical confounder criteria (R2* > 35 s^{-1} or ALT > 2.5× ULN); when broader phenotypic features (heterogeneity, lean MAFLD, mixed pathology) are added, the prevalence of "complex" MAFLD presentations approaches the 25–30% range reported in larger tertiary cohorts [9,22].

5.4. Clinical Implications

Three implications follow for practice:

• Where the clinical question is "does this patient have any MAFLD?" (≥5% threshold), all three methods perform adequately at the population level (AUROC > 0.96), and any can reasonably be used for screening [9,13].

• Where the clinical question is "what grade of steatosis does this patient have and is it changing under treatment?", systematic biases of ±8–10 percentage points are unacceptable. True UDFF is the only method tested here that delivers grade-level accuracy ($\varkappa$ = 0.98) suitable for serial monitoring and trial endpoints [4,28].

• In patients with elevated ferritin, transferrin saturation, ALT > 2× ULN, or BMI < 25 with metabolic risk factors, single-parameter methods (Sequoia UDFF, ATI) should be interpreted with caution and confirmed by either True UDFF or MRI-PDFF before treatment escalation [17,18,21–23].

5.5. Limitations

This analysis uses a 270-patient single-cohort dataset and relies on derived MRI-PDFF values for the reference standard. Histological correlation, inter-operator variability, longitudinal performance, and external validation in independent centres remain to be established [25,26]. The ATI-to-fat-percentage conversion used the published linear formula (Fat% = (ATI − 0.41) × 33.33) [13], and a non-linear or vendor-specific conversion may shift the absolute ATI bias somewhat — but is unlikely to eliminate the systematic offset shown in Section 3.3, which is driven by the underlying single-parameter physics rather than the conversion equation. Finally, "True UDFF" here refers specifically to the FibroPlus/ULFI prototype; other multi-parametric implementations may differ in their confounder-correction models [14,16].

6. Conclusions

In 270 paired measurements, True UDFF (multi-parametric, with explicit iron and inflammation correction) outperformed both Sequoia UDFF (single-pass calibrated) and ATI (single attenuation coefficient) in every metric of clinical relevance: correlation with MRI-PDFF (r = 0.995 vs 0.951 and 0.975), Bland–Altman bias (≈0% vs +8.2% and −9.8%), AUROC at ≥17% steatosis (0.999 vs 0.978 and 0.992), and steatosis-grade agreement ($\varkappa$ = 0.98 vs 0.68 and 0.52). The performance gap widens sharply in the 19% of patients meeting clinical confounder criteria (R2* > 35 s^{-1} or ALT > 2.5× ULN), where the Sequoia bias rises to +10–12% and the ATI bias remains around −9%, while True UDFF's mean absolute error stays under 1%.

Population-level calibration of single-parameter QUS methods is sufficient for screening but not for individual-level quantification, severity grading, treatment monitoring, or trial endpoints — exactly the use cases driving the current expansion of MAFLD imaging. Multi-parametric True UDFF, by combining backscatter, speed of sound, and attenuation features with an explicit confounder-correction model, closes the gap to MRI-PDFF for these higher-stakes applications, and additionally identifies the complex phenotypes (mixed, lean, masked steatosis) that single-parameter methods cannot detect.

7. Acknowledgements

We thank the imaging and research staff who supported acquisition of the FibroPlus dataset, and the study participants who consented to multiparametric ultrasound and MRI examinations. Funding: institutional research support; no commercial sponsor. Conflicts of interest: none declared. Author contributions: study design, data analysis, manuscript drafting and revision per ICMJE criteria.

References

1. Eslam M, Newsome PN, Sarin SK, Anstee QM, Targher G. A new definition for metabolic dysfunction-associated fatty liver disease: an international expert consensus statement. J Hepatol. 2020; 73(1): 202-209.
2. Eslam M, Sanyal AJ, George J; International Consensus Panel. MAFLD: a consensus-driven proposed nomenclature for metabolic associated fatty liver disease. Gastroenterology. 2020; 158(7): 1999-2014.e1.
3. Younossi ZM, Koenig AB, Abdelatif D, Fazel Y, Henry L, Wymer M. Global epidemiology of nonalcoholic fatty liver disease — meta-analytic assessment of prevalence, incidence, and outcomes. Hepatology. 2016; 64(1): 73-84.
4. Younossi ZM, Golabi P, Paik JM, Henry A, Van Dongen C, Henry L. The global epidemiology of nonalcoholic fatty liver disease (NAFLD) and nonalcoholic steatohepatitis (NASH): a systematic review. Hepatology. 2023; 77(4): 1335-1347.
5. Reeder SB, Sirlin CB. Quantification of liver fat with magnetic resonance imaging. Magn Reson Imaging Clin N Am. 2010; 18(3): 337-357.
6. Reeder SB, Cruite I, Hamilton G, Sirlin CB. Quantitative assessment of liver fat with magnetic resonance imaging and spectroscopy. J Magn Reson Imaging. 2011; 34(4): 729-749.
7. Caussy C, Reeder SB, Sirlin CB, Loomba R. Non-invasive, quantitative assessment of liver fat by MRI-PDFF as an endpoint in NASH trials. Hepatology. 2018; 68(2): 763-772.
8. Ferraioli G, Soares Monteiro LB. Ultrasound-based techniques for the diagnosis of liver steatosis. World J Gastroenterol. 2019; 25(40): 6053-6062.
9. Ferraioli G, Kumar V, Ozturk A, Nam K, de Korte CL, Barr RG. US attenuation for liver fat quantification: an AIUM-RSNA QIBA pulse-echo quantitative ultrasound initiative. Radiology. 2022; 302(3): 495-506.
10. Labyed Y, Milkowski A. Novel method for ultrasound-derived fat fraction using an integrated phantom. J Ultrasound Med. 2020; 39(12): 2427-2438.
11. Kubale R, Schneider G, Lessenich CPN, Buecker A, Massmann A. Ultrasound-derived fat fraction for hepatic steatosis assessment: prospective study of agreement with MRI-PDFF and sources of variability in a heterogeneous population. AJR Am J Roentgenol. 2024; 222(4): e2330775.
12. Bae JS, Lee DH, Lee JY, Kim H, Yu SJ. Assessment of hepatic steatosis by using attenuation imaging: a quantitative, easy-to-perform ultrasound technique. Eur Radiol. 2019; 29(12): 6499-6507.
13. Dioguardi Burgio M, Ronot M, Reizine E, Rautou PE, Castera L. Quantification of hepatic steatosis with ultrasound: promising role

of attenuation imaging coefficient in a biopsy-proven cohort. Eur Radiol. 2020; 30(4): 2293-2301.

14. Han A, Andre MP, Deiranieh L, Housman E, Erdman JW Jr, Loomba R, et al. Repeatability and reproducibility of the ultrasonic attenuation coefficient and backscatter coefficient measured in the right lobe of the liver in adults with known or suspected non-alcoholic fatty liver disease. J Ultrasound Med. 2018; 37(8): 1913-1927.
15. Lin SC, Heba E, Wolfson T, Ang B, Gamst A. Noninvasive diagnosis of nonalcoholic fatty liver disease and quantification of liver fat using a new quantitative ultrasound technique. Clin Gastroenterol Hepatol. 2015; 13(7): 1337-1345.e6.
16. Han A, Boehringer AS, Zhang YN, Hooker JC, Andre MP. Inter-platform reproducibility of ultrasonic attenuation and backscatter coefficients in assessing NAFLD. Eur Radiol. 2019; 29(9): 4699-4708.
17. Ryan JD, Armitage AE, Cobbold JF, Banerjee R, Borsani O. Hepatic iron is the major determinant of serum ferritin in NAFLD patients. Liver Int. 2018; 38(1): 164-173.
18. Valenti L, Fracanzani AL, Bugianesi E, Dongiovanni P, Galmozzi E. HFE genotype, parenchymal iron accumulation, and liver fibrosis in patients with nonalcoholic fatty liver disease. Gastroenterology. 2010; 138(3): 905-912.
19. Brunt EM, Kleiner DE, Wilson LA, Belt P, Neuschwander-Tetri BA; NASH Clinical Research Network. Nonalcoholic fatty liver disease (NAFLD) activity score and the histopathologic diagnosis in NAFLD: distinct clinicopathologic meanings. Hepatology. 2011; 53(3): 810-820.
20. Capitan V, Petit JM, Aho S, Lefevre PH, Favelier S. Macroscopic heterogeneity of liver fat: an MR-based study in type-2 diabetic patients. Eur Radiol. 2012; 22(10): 2161-2168.
21. Younes R, Bugianesi E. NASH in lean individuals. Semin Liver Dis. 2019; 39(1): 86-95.
22. Kumar R, Priyadarshi RN, Anand U. Non-obese NAFLD: a distinct entity driven by dysmetabolism. Hepatol Int. 2023; 17(1): 23-35.
23. Nelson JE, Wilson L, Brunt EM, Yeh MM, Kleiner DE. NASH Clinical Research Network. Relationship between the pattern of hepatic iron deposition and histological severity in nonalcoholic fatty liver disease. Hepatology. 2011; 53(2): 448-457.
24. De Robertis R, Spoto F, Autelitano D, Guagenti D, Olivieri A. Ultrasound-derived fat fraction for detection of hepatic steatosis and quantification of liver fat content. Radiol Med. 2023; 128(11): 1383-1390.
25. Hu Y, Zhou J, Wang X, Wang Y, Chen Y. Comparing ultrasound-derived fat fraction and MRI-PDFF for quantifying hepatic steatosis: a real-world prospective study. Eur Radiol. 2025; 35(4): 2156-2166.
26. Yoo J, Lee JM, Joo I, Lee DH, Yoon JH, Kang HJ, Ahn SJ. Reproducibility of ultrasound attenuation imaging for the noninvasive evaluation of hepatic steatosis. Ultrasonography. 2020; 39(2): 121-129.
27. Karlas T, Petroff D, Sasso M, Fan JG, Mi YQ. Individual patient data meta-analysis of controlled attenuation parameter (CAP) technology for assessing steatosis. J Hepatol. 2017; 66(5): 1022-1030.
28. Castera L, Friedrich-Rust M, Loomba R. Noninvasive assessment of liver disease in patients with nonalcoholic fatty liver disease. Gastroenterology. 2019; 156(5): 1264-1281.e4.
29. Tang A, Tan J, Sun M, Hamilton G, Bydder M. Nonalcoholic fatty liver disease: MR imaging of liver proton density fat fraction to assess hepatic steatosis. Radiology. 2013; 267(2): 422-431.
30. Loomba R, Neuschwander-Tetri BA, Sanyal A, Chalasani N. Multicenter validation of association between decline in MRI-PDFF and histologic response in NASH. Hepatology. 2020; 72(4): 1219-1229.